AD-752 591

FIREBALL ENTRAINMENT STUDY

Wayne W. Haigh, et al

TRW Systems Group

Prepared for:

Advanced Research Projects Agency

August 1972

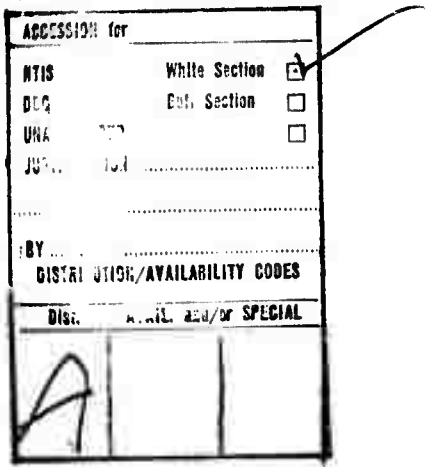

When this report is no longer needed, Department of Defense Organizations will destroy it in accordance with appropriate procedures. Contractors will destroy the report according to the requirements of the Industrial Security Manual for safeguarding classified information.

Retention of this document by DoD Contractors is authorized in accordance with Paragraph 2, Industrial Security Letter 71L-3, dated 17 May 1971.

Unclassified
Security Classification

AD-752591

DOCUMENT CONTROL DATA - R&D
(Security classification of title, body of abstract and indexing annotation must be entered when the overall report is classified)

1 ORIGINATING ACTIVITY (Corporate author)
TRW Systems Group
One Space Park
Redondo Beach, California 90278

2a REPORT SECURITY CLASSIFICATION
Unclassified

2b GROUP

3 REPORT TITLE
FIREBALL ENTRAINMENT STUDY

4 DESCRIPTIVE NOTES (Type of report and inclusive dates)
Semi-Annual Report - 15 January 1972 to 31 August 1972

5 AUTHOR(S) (Last name, first name, initial)
Haigh, Wayne, W. and Mantrom, David, D.

6 REPORT DATE	7a TOTAL NO OF PAGES	7b NO OF REFS
August 1972	59	17

8a CONTRACT OR GRANT NO	9a ORIGINATOR'S REPORT NUMBER(S)
DNA 001-72-C-0019	18895-6002-RO-00
b PROJECT NO ARPA Order No. 1433	
c Work Unit No. 08 d Program Code No. 1E50	9b OTHER REPORT NO(S) (Any other numbers that may be assigned this report) DNA 2981Z

10 AVAILABILITY/LIMITATION NOTICES
Approved for public release; distribution unlimited.

11 SUPPLEMENTARY NOTES	12 SPONSORING MILITARY ACTIVITY
	Director Advanced Research Projects Agency Washington, D. C. 20301

13 ABSTRACT

An experimental program to study the process of entrainment and turbulent mixing in fireballs is described. The high pressure test facility and diagnostic equipment which were developed for this investigation and preliminary analyses which have been performed are discussed. Methods of acquiring density and velocity field data using holographic interferometry and particle tracking techniques, respectively, as well as the interpretation and reduction of these data are outlined. Preliminary experimental results obtained at tank pressures of four and eight atmospheres are presented.

DD FORM 1 JAN 64 1473

Unclassified
Security Classification

Unclassified

Security Classification

14 KEY WORDS	LINK A		LINK B		LINK C	
	ROLE	WT	ROLE	WT	ROLE	WT
Entrainment						
Fireballs						
Turbulent Mixing						
Holographic Interferometry						
Fireball Experiments						

INSTRUCTIONS

1. ORIGINATING ACTIVITY: Enter the name and address of the contractor, subcontractor, grantee, Department of Defense activity or other organization *(corporate author)* issuing the report.

2a. REPORT SECURITY CLASSIFICATION: Enter the overall security classification of the report. Indicate whether "Restricted Data" is included. Marking is to be in accordance with appropriate security regulations.

2b. GROUP: Automatic downgrading is specified in DoD Directive 5200.10 and Armed Forces Industrial Manual. Enter the group number. Also, when applicable, show that optional markings have been used for Group 3 and Group 4 as authorized.

3. REPORT TITLE: Enter the complete report title in all capital letters. Titles in all cases should be unclassified. If a meaningful title cannot be selected without classification, show title classification in all capitals in parenthesis immediately following the title.

4. DESCRIPTIVE NOTES: If appropriate, enter the type of report, e.g., interim, progress, summary, annual, or final. Give the inclusive dates when a specific reporting period is covered.

5. AUTHOR(S): Enter the name(s) of author(s) as shown on or in the report. Enter last name, first name, middle initial. If military, show rank and branch of service. The name of the principal author is an absolute minimum requirement.

6. REPORT DATE: Enter the date of the report as day, month, year, or month, year. If more than one date appears on the report, use date of publication.

7a. TOTAL NUMBER OF PAGES: The total page count should follow normal pagination procedures, i.e., enter the number of pages containing information.

7b. NUMBER OF REFERENCES: Enter the total number of references cited in the report.

8a. CONTRACT OR GRANT NUMBER: If appropriate, enter the applicable number of the contract or grant under which the report was written.

8b, 8c, & 8d. PROJECT NUMBER: Enter the appropriate military department identification, such as project number, subproject number, system numbers, task number, etc.

9a. ORIGINATOR'S REPORT NUMBER(S): Enter the official report number by which the document will be identified and controlled by the originating activity. This number must be unique to this report.

9b. OTHER REPORT NUMBER(S): If the report has been assigned any other report numbers *(either by the originator or by the sponsor)*, also enter this number(s).

10. AVAILABILITY/LIMITATION NOTICES: Enter any limitations on further dissemination of the report, other than those imposed by security classification, using standard statements such as:

(1) "Qualified requesters may obtain copies of this report from DDC."

(2) "Foreign announcement and dissemination of this report by DDC is not authorized."

(3) "U. S. Government agencies may obtain copies of this report directly from DDC. Other qualified DDC users shall request through _____."

(4) "U. S. military agencies may obtain copies of this report directly from DDC. Other qualified users shall request through _____."

(5) "All distribution of this report is controlled. Qualified DDC users shall request through _____."

If the report has been furnished to the Office of Technical Services, Department of Commerce, for sale to the public, indicate this fact and enter the price, if known.

11. SUPPLEMENTARY NOTES: Use for additional explanatory notes.

12. SPONSORING MILITARY ACTIVITY: Enter the name of the departmental project office or laboratory sponsoring *(paying for)* the research and development. Include address.

13 ABSTRACT: Enter an abstract giving a brief and factual summary of the document indicative of the report, even though it may also appear elsewhere in the body of the technical report. If additional space is required, a continuation sheet shall be attached.

It is highly desirable that the abstract of classified reports be unclassified. Each paragraph of the abstract shall end with an indication of the military security classification of the information in the paragraph, represented as *(TS). (S). (C). or (U)*

There is no limitation on the length of the abstract. However, the suggested length is from 150 to 225 words.

14 KEY WORDS: Key words are technically meaningful terms or short phrases that characterize a report and may be used as index entries for cataloging the report. Key words must be selected so that no security classification is required. Identifiers, such as equipment model designation, trade name, military project code name, geographic location, may be used as key words but will be followed by an indication of technical context. The assignment of links, rules, and weights is optional.

Unclassified

Security Classification

Ia

AD-752 591

18895-6002-R0-00

DNA 2981Z

FIREBALL ENTRAINMENT STUDY
SEMI-ANNUAL REPORT

This work was supported by the
Defense Nuclear Agency under
subtask ARPA ZL433-08.

August 1972

ARPA Order No. 1433
Program Code No. 1E50
Work Unit No. 08
Contractor - TRW, Incorporated
Dates of Contract - 8/18/71 - 9/30/72
Contract Amount - $134,870
Short Title: Fireball Entrainment

Contract No. DNA 001-72-C-0019
Principal Investigator -
Dr. John E. Lewis
Telephone No.: (213) 536-4422
Project Engineer - Wayne W. Haigh
Telephone No.: (213) 535-2792
Sales No.: 18895

TRW SYSTEMS GROUP

ib

FOREWORD

This research was supported by the Advanced Research Projects Agency and was monitored by the Defense Nuclear Agency, under ARPA Order No. 1433 and Contract DNA 001-72-C-0019.

The views and conclusions contained in this document are those of the authors and should not be interpreted as necessarily representing the official policies, either expressed or implied, of the Advanced Research Projects Agency or the U. S. Government.

CONTENTS

ILLUSTRATIONS

1. INTRODUCTION

This report describes the initial phase of a program which ultimately will allow the reliable prediction of chemical species and temperature within the atmosphere following a low altitude nuclear explosion. The development of fireballs from low yield (<100 kton) bursts at these altitudes (<30 km), of direct concern to Site Defense, will be dominated by buoyancy forces. The initial stage of these fireballs resulting from large energy release within the atmosphere is characterized by spherical symmetry, the domination of radiative energy transport, and the propagation of a strong spherical shock wave. Approximately one second after detonation, the fireball comes to pressure equilibrium with the ambient air and because of its low density, begins to rise. As the fireball rises, circulation is generated and a toroid is formed. The series of laboratory experiments currently being performed are designed to simulate these "buoyant rise" fireballs after pressure equilibration.

The reliable prediction of both radar and optical signatures resulting from atmospheric nuclear detonations is an important and necessary prerequisite for a defense system design and evaluation. Before such signatures can be predicted, the resulting spatial distribution of temperature and chemical composition must be known and this requires a reliable theoretical entrainment model. At present, no data exists for the validation of such modeling. Optical data from nuclear tests give only gross features of the events such as fireball size and rise, but what is required is a knowledge of the temperature, species, and velocity fields. This experimental study will establish a sound physical data base to support the development and evaluation of theoretical mixing and entrainment models.

2. SUPPORT ANALYSIS

A phenomenological model of a rising fireball or, more generally, an isolated buoyant mass has been developed. The main emphasis in development of this model was oriented toward, although not limited to, a supporting role in the design and development of the experimental fireball simulation facility. For this reason and because most of the physics of the various details of the fireball behavior (such as the entrainment of external fluid and subsequent turbulent mixing) are not well understood, the approach taken was to satisfy in an integrated sense the various conservation laws of mass, momentum and energy.

A recent paper by Wang (Reference 1) presented an analogous derivation to the present approach as have Morton, G. I. Taylor and Turner in Reference 2 for very small density differences. These papers, as important and informative as they are, are not necessarily applicable to either the fireball or the laboratory case under investigation here. In the latter analyses the effects of different species are not contained whereas in the former a similar situation prevails along with the fact that atmospheric scale height effects are not included.

The purpose of this analysis has been to extend these works to include these phenomena. A discussion and derivation of this model is given below.

2.1 GENERAL REMARKS

Consider a generally spherical region with density ρ_i formed within an external atmosphere with a larger density ρ_∞. This spherical mass will rise initially with an acceleration of 2g's because of the coupled density difference and gravitational field. Observations (e.g., Reference 3) indicate that this acceleration does not continue indefinitely because of two effects. The first of these is that the low density region undergoes a geometric change and forms into a torus after a translation of approximately one initial diameter. Commensurate with this geometric change, the buoyant region begins entraining external fluid at a greatly enhanced rate and thus the mass of fluid carried with the torus increases significantly (the

buoyant force also diminishes for displacements on the order of a scale height). It is this phase of fireball development that is treated here since during this stage, the degree of turbulent mixing and entrainment of cool air into the fireball will establish the temperatures and chemical species present for the third or final stage of the fireball history, the "pancaking" about the stabilization altitude.

After the initial torus formation stage, it is necessary for mathematical simplicity to assume that the fireball is similarly shaped during the period of interest. The fact that this is approximately correct is given by field data in classified reports as well as by simple experiments (see Reference 4 for instance). From these latter measurements, it is also evident that the fireball (here we are talking about the entire region carried along with the initial products) is roughly spherical in shape. Thus, the fireball surface area and volume can be characterized by a single parameter 'a' which can be thought of as the radius of a sphere of the same volume.

2.2 EQUATIONS OF MOTION

The continuity or entrainment equation is assumed to be of the form

$$\frac{dm_a}{dt} = \alpha \rho_\infty u(4\pi a^2) \tag{1}$$

where m_a is the mass of entrained atmospheric air

$\rho_\infty(z)$ is the atmospheric density

u is the rise velocity of the fireball center

$4\pi a^2$ is the surface area of the equivalent sphere

α is the dimensionless entrainment rate which is assumed constant

We can also define average densities ρ_a and ρ_i from

$$\rho_a = \frac{m_a}{(4/3)\pi a^3} \tag{2a}$$

$$\text{and} \qquad \rho_i = \frac{m_i}{(4/3)\pi a^3} \tag{2b}$$

where m_i refers to the initial mass of the fireball and is a given constant. Obviously, the average fireball density is given as

$$\rho = \rho_a + \rho_i \tag{3}$$

The equation of motion for the fireball is

$$\frac{4}{3}\pi a^3(\rho + \frac{1}{2}\rho_\infty)\frac{du}{dt} = \frac{4}{3}\pi a^3(\rho_\infty - \rho)g - C_D(\frac{1}{2}\rho_\infty u^2)(\pi a^2) \tag{4}$$

The term $\frac{1}{2}\rho_\infty$ within the parentheses on the LHS of equation (4) accounts for the "apparent mass" effect or the additional inertia caused by accelerating a spherical object in an inviscid fluid. The RHS is simply the buoyant force less the drag force. The drag coefficient C_D includes both the form drag C_D' and the entrainment drag given by 8α. It is assumed that C_D' is constant. This assumption is not critical in that it will be shown that the form drag is small compared to the entrainment drag.

The final consideration which will form a complete system is the energy equation. To formulate this to the same degree of approximation as the previous equations it is assumed that the pressure within the fireball is uniform and is equal to the ambient pressure at the center elevation of the fireball. This assumption does become weaker for fireball dimensions on the order of an atmospheric scale height ($\sim$8km). Further, it is assumed that the kinetic energy is small compared with the thermal or potential energy of the fireball (this ratio is on the order of $u^2/\gamma RT_\infty$ which is small). The total enthalpy within the fireball is then:

$$H_t = \frac{4}{3}\pi a^3(\rho_i c_{pi} + \rho_a c_{pa})T \tag{5}$$

where c_{pi} and c_{pa} are the specific heats of the initial mass and the entrained air, respectively.

For moderate pressures and temperatures, the perfect gas equation of state then permits this to be written as:

$$H_t = \frac{4}{3}\pi a^3 p_\infty \frac{\bar{c}_p}{\bar{R}} \tag{6}$$

where the mass concentrations are defined as

$$C_i = \frac{\rho_i}{\rho} = \frac{m_i}{m_i + m_a} \; ; \; C_a = \frac{\rho_a}{\rho} = \frac{m_a}{m_i + m_a} \tag{7}$$

and the average specific heat and gas constant are, respectively:

$$\begin{aligned} \bar{c}_p &= C_i c_{pi} + C_a c_{pa} \\ \bar{R} &= C_i R_i + C_a R_a \end{aligned} \tag{8}$$

The rate of change of the total enthalpy is then given from the Second Law of Thermodynamics and assuming that the entrainment and mixing are adiabatic over the entirety of the fireball. Thus,

$$\frac{dH_t}{dt} = c_{pa} T_a \frac{dm_a}{dt} + \left(\frac{4}{3}\pi a^3\right) \frac{dp_\infty}{dt} \tag{9}$$

The second term on the RHS accounts for the fact that the ambient pressure varies with fireball position or time. This variation is approximated by assuming that locally the pressure-altitude dependence is given by:

$$\frac{1}{p_\infty} \frac{dp_\infty}{dz} = \frac{1}{L} \tag{10}$$

where L is termed the pressure scale height and is a slowly varying function of altitude (e.g., $L \sim 8.7$km at sea level and $L \sim 6.9$km at 30km altitude).

Differentiating equation (6) and equating it to equation (9) yields after some algebra

$$\frac{da}{dt} = -\frac{1}{3}\frac{au}{\gamma L} + \alpha u A \tag{11}$$

where

$$A = \frac{c_{pa}\bar{R}}{\bar{c}_p R_a} + \frac{R_a/\bar{R} - c_{pa}/\bar{c}_p}{\rho/\rho_\infty} \tag{12}$$

Thus, the full set of differential equations which describe the evolution of the fireball are:

$$\frac{dm_a}{dt} = \alpha(4\pi a^2)\rho_\infty u$$

$$\frac{du}{dt} = \frac{(\rho_\infty - \rho_a - \rho_i)g - \frac{3}{8} C_D \rho_\infty u^2/a}{(\frac{1}{2}\rho_\infty + \rho_a + \rho_i)} \tag{13}$$

$$\frac{da}{dt} = -\frac{1}{3}\frac{au}{\gamma L} + \alpha u A$$

These equations can be easily integrated numerically subject to the initial conditions at $t = t_o$ that

$$a = a_o,\ u = u_o,\ \rho_a = 0,\ \rho_{i_o} = \frac{m_i}{(4/3)\pi a_o^3} \tag{14}$$

and the algebraic relations

$$\rho_i = \rho_{i_o}\left(\frac{a_o}{a}\right)^3 \text{ and } C_D = C_D' + 8\alpha \tag{15}$$

The determination of the initial fireball radius, a_o can be ascertained from either experimental data or, in the case of a nuclear explosion, estimated from the yield, Y (in kilotons) and the atmospheric density at burst height, ρ_∞ (in kg/m^3). An example of such an expression taken from Reference 5 is:

$$a_o = 0.12\left(\frac{Y}{\rho_\infty}\right)^{1/3} \text{ km}$$

The "initial" velocity u_o is not taken as zero inasmuch as this analysis is only intended for times after torus formation. Although the net displacement of the fireball is small [$O(a_o)$] the vertical velocity at this location is not negligible. Investigations as to how to estimate this are still underway. Preliminary indications, however, suggest that torus formation occurs when

$$u_o \sim 0.4u_T = 0.4\sqrt{\frac{8}{3}\frac{ga_o}{C_D}\left(\frac{\rho_\infty - \rho i_o}{\rho_\infty}\right)} \qquad (16)$$

where u_T is the terminal velocity of a nonentraining sphere.

One last parameter that must be estimated before a solution can be obtained is the entrainment constant α. Recourse to available experimental data is necessary to determine this quantity in lieu of the fact that a theoretical estimate is not available from existing turbulent entrainment theories. The most straightforward estimate of α can be obtained from the experimental data for the fireball size as a function of position. From the last of equations (13) the spatial derivative of the fireball size is given by

$$\frac{da}{dz} = -\frac{a}{3\gamma L} + \alpha A \qquad (17)$$

where the fact that $u = \frac{dz}{dt}$ has been used.

If only one species is involved, the quantity A is identically one (even for two species mixtures it is found that the entrained mass far overwhelms the initial mass so that this approximation is also valid). Note that in equation (17) the growth rate is effected by scale height in addition to the usual entrainment growth rate.

Data from small scale helium release experiments in Reference 6 showed a range of values for α from 0.08 to 0.18 with an average of 0.12. Similar preliminary experiments were performed as part of this study which yielded values for α from 0.10 to 0.15 with an average value of 0.125.

Field test data from nuclear tests show typical values for α to vary from 0.13 to 0.26 if atmospheric scale height effects are accounted for. The enormous variation in scale between the experiments and the field data should not be overlooked here--the nuclear explosions are some 100,000 times larger than the experiments. A similar variation in Reynolds number is also noted (10^4 for the lab compared to 10^9 or 10^{10} for nuclear explosions). In spite of this, the small variation in the entrainment constant α which is, at most, a factor of two over the entire range of Reynolds number is indeed gratifying although the size effect is not completely removed.

The spherical form drag coefficient C_D' for Reynolds numbers 10^4 is roughly on the order of 0.2 or lower. Comparing this to the "entrainment drag" coefficient 8α shows that the form drag is less than 10% of the total drag given in equation (15). Thus the variation in C_D' with Reynolds number is relatively unimportant insofar as the dynamics of the fireball is concerned.

One additional feature of the solution to these equations is the prediction of the stabilization altitude. This is the altitude where the fireball eventually comes to rest (actually the fireball oscillates about this altitude at roughly the Brunt-Väsäilä frequency $\omega = [\frac{g}{\rho_\infty} \frac{d\rho_\infty}{dz}]^{1/2}$). Thus, the solutions are valid up to the time where the "collapse" of the spherical region by differential buoyant forces becomes significant. For nuclear events, this is on the order of tens of minutes.

The equations of motion of the fireball derived in this section have been programmed for numerical integration and will be used to provide theoretical results for comparison with both laboratory and field data. Additional future work in this area will be to examine these data to improve estimates of the initial conditions (t_o, u_o, a_o).

It should be emphasized again that the primary purpose of this fireball analysis is to support the experimental study. A sophisticated 2-dimensional time dependent code, well beyond the scope of the present program, would be required to incorporate the turbulent mixing and entrainment models (as derived from the experiments for example) and predict the distribution of chemical species and temperature within the atmosphere following a nuclear explosion.

3. EXPERIMENTAL FACILITY

A test facility consisting of several primary components including a high pressure test tank with optical ports, a pressurization and exhaust system for the tank, equipment for the remote formation and controlled bursting of helium-filled soap bubbles, and the necessary diagnostic equipment to obtain density and velocity field measurements have been designed, developed, and tested.

3.1 HIGH PRESSURE TANK AND AUXILIARY EQUIPMENT

The high pressure tank is an ASME pressure vessel with a diameter of 54 inches and a length of 14 feet. A photograph of the test tank installed in the TRW Fluid Mechanics Laboratory is shown in Figure 1. This facility was designed to operate in a pressure range from vacuum conditions to 10 atmospheres.

Viewing ports were designed to provide a 12 inch diameter horizontal view and a 10 inch diameter vertical view. The horizontal view ports are located 10 inches above the tank centerline to allow torus vertical trajectories of 15 bubble diameters (based on an initial soap bubble diameter of 2 inches) without significant wall interference.

The high pressure tank is equipped with both a pressurization and venting system. Tank venting is accomplished through a symmetrical duct system consisting of 4 inch diameter flanges on each end of the tank which are piped to a common high-speed valve and muffler system outside the building. The symmetrical vent system and control valve are shown in Figure 1. The high pressure tank was designed symmetrically and with a length-to-diameter ratio of about 3 to minimize induced velocities on the torus motion during tank venting. The vent control valve is a 6 inch diameter, pneumatically actuated, Lunkenheimer ball valve which will allow the tank pressure to be reduced from 10 to 2 atmospheres in about 2 seconds. High pressure nitrogen bottles manifolded together are used to pressurize the tank.

A system was designed and developed to remotely form and burst helium-filled soap bubbles in the high pressure tank. Positive displacement pistons and a valving system are used to meter the amount of helium and soap solution to the bubble tube to accurately control the bubble size. A small electrode spaced about 20 mils from the bubble tube has been used with a 200 microfarad capacitor discharge system to repeatedly burst the bubbles. Several other methods of bursting the bubbles are currently being investigated to improve if possible the symmetry of the initial helium release. The bubble formation head and present electrode breaker have been designed as an integral unit so they can be traversed vertically within the tank through a 1 inch diameter access flange and seal. The bubble tube position can be varied from the center to 30 inches below the horizontal viewing ports.

3.2 DIAGNOSTIC EQUIPMENT

In order to completely specify the fluid state and motion the following must be known for a non-reacting gas: two thermodynamic variables, such as pressure and temperature; a variable of the motion, such as velocity; and the composition of the field. Measurements of the tank pressure and temperature, outside the induced flow, suffice for specifying the pressure and temperature of the field since the induced fluid motion is incompressible (i.e., low velocity and adiabatic). The remaining unknowns, density (or composition) and velocity are measured optically using holographic interferometry and a particle tracking technique, respectively. Optical techniques were adopted for this study because of three primary difficulties involved with flow field probes. First, interpretation of data obtained from probes in a highly three-dimensional flow is almost impossible. Also, probe interference effects are sizable in an incompressible flow such as this, and finally the cost and time consumed in reconstructing a time dependent flow field from local measurements are prohibitive.

3.2.1 Holographic Interferometer

Pulsed laser holographic interferometry will be used to measure the mean density field and turbulent structure of the rising toroids. This technique has been used extensively at TRW to measure mean and turbulent flow field properties of wakes as described in Reference 7. The laser holograph* which will be used in this program is similar in design to the one used in previous studies but has been considerably increased in size to accommodate the large high pressure tank. The main feature of the holocamera is that it records orthogonal views simultaneously across the tank test section. Consequently, this system is capable of recording any transmission subject in a 9 inch diameter area in line with the 8 by 10 inch photographic plates and the large 18 inch objective lens at the opposite ports. The advantages of using this holographic interferometer as compared to the standard Mach Zehnder interferometer include the three-dimensional viewing and depth focusing properties of holographic interferograms, and the fact that precision optics and accurate alignment are not required with holographic interferometry since a common optical path is used for both the scene and comparison beams. An end view of the tank and ports and holocamera components in close proximity to the tank are shown in Figure 2 while a schematic of the complete holocamera identifying all primary optical components is presented in Figure 3. A photograph of the holocamera together with the test tank is shown in Figure 4.

In this holocamera the primary beam for the laser is split into a reference and a scene beam. The scene beam is directed through the scene to the plates whereas the reference beam is directed on the plates without passing through the disturbance. The prism plate and lenses shown in Figure 3 are used to spatially and temporally match the scene and reference beams over the plates. A Q-switched solid state ruby laser with an energy of about 1 joule and pulse length of about 100 nanoseconds is used to expose both the vertical and horizontal beam holograms which are recorded on Agfa-Gavaert 8E75 plates.

*The term laser holograph pertains to both the laser cavity or oscillator, and all other optical components which comprise the holocamera.

Interferograms are obtained in this common path interferometer by sequentially recording the comparison and scene beams on the same plates. The double exposure of the plates by the two pulses, the one of the undisturbed volume and the other of the same volume with the test scene introduced, produces the interferograms. The standard mode of operation of this holocamera in which the position of all optical components remain fixed during the time between the two exposures produces an interference record called an infinite fringe interferogram. A very small, accurately controlled rotation of a mirror and the corresponding plate between the two exposures, will yield a different type of interference pattern on the plate called a finite fringe interferogram. The hardware necessary to permit this accurate rotation of optical components has been designed and fabricated for the holocamera horizontal beam and will be used throughout the study as necessary. A discussion of the interpretation of both finite and infinite fringe interferograms and the advantages and disadvantages of each is included in Section 4.2.

3.2.2 Particle Tracking Apparatus

The fluid velocity will be measured by photographically recording the motion of tracer particles which follow the fluid motion. Provided that the particle Reynolds number based on lag velocity and particle diameter is less than about 1, the drag force is viscous rather than inertia dominated, and the particles will quickly attain and follow the fluid motion. An exhaustive treatment of using particulate tracers for fluid velocity measurements was conducted in a wind tunnel by Bourot as described in Reference 8. More recently, flow visualization studies have successfully been conducted utilizing light reflection from small helium-filled soap bubbles as indicated in Reference 9. During the course of this recent work, equipment was developed by Sage Action, Inc. (SAI) which could continuously produce helium-filled soap bubbles as tracer particles with various degrees of buoyancy.

An SAI Model 3 console and low speed bubble head will be used in the current program to produce slightly buoyant bubbles about 1/8 inch in

diameter. The bubble head will be mounted at the bottom of the test tank on a traversing mechanism so a vertical sheet of bubbles about 10 inches long will be produced along the tank axis.

A 1500 watt tungsten-halogen lamp rated at 30,000 lumens will be attached above the top view port and masked to produce a high intensity light beam 1/4 inch wide by about 10 inches long coincident with the sheet of bubbles. A 4 by 5 inch view camera will be mounted at one of the side windows and focused on the light sheet to record the motion of all illuminated bubbles in the field of view. A minimum of three multiple exposures will be obtained in each test run with an exposure time of about 100 msec using a MATI electroshutter. Each film record will show a particle trajectory as a row of dashes the lengths of which will be used to determine the local velocity at that point in the field. Velocity data will only be reduced from central dashes in each particle trajectory since the initial and final dash in a trajectory could be produced with a particle either entering or leaving the light beam during the exposure.

4. DATA ACQUISITION AND INTERPRETATION

The purpose of this section is to discuss both the procedure for obtaining holographic interferograms and the physical interpretation of this form of data. Acquisition of velocity field data with the particle tracking apparatus was discussed previously in Section 3.2.2.

4.1 ACQUISITION OF INTERFEROMETRY DATA

The procedure which is used to obtain an orthogonal set of infinite fringe interferograms of a simulated fireball consists of the following primary steps:

1. Plate holders containing the special fine grain, low speed photographic plates are loaded in the horizontal and vertical plate holder receptacles.

2. The slides covering the plates are drawn after the laser and bubble blowing apparatus have been checked and all sources of illumination in the test area have been eliminated.

3. A helium-filled soap bubble is blown to a predetermined size and the laser power supply is charged.

4. About five seconds after its formation, the helium bubble is burst.

5. Simultaneous with the bubble bursting, an electrical signal, first sent to a time delay circuit, activates the laser firing mechanism which records the test scene on the plates. The time delay is adjusted to allow the helium cloud to rise to near the center of the windows. A typical time delay of 650 milliseconds would allow a bubble with an initial diameter of one inch to rise about five inches at a tank pressure of eight atmospheres.

6. A comparison scene is recorded on the plates by firing the laser a second time about 30 seconds after the event scene. This delay ensures that the disturbance is well outside of the viewing region resulting in a uniform, constant density comparison scene.

7. The photographic plates are removed and developed using special photographic developing agents.

8. The holograms are reconstructed, i.e., observed and photographed by illuminating the holograms with a cw laser.

9. Large scale working photographs are now produced for use in the data reduction phase as described in Section 5.1.3.

A horizontal view finite fringe interferogram is obtained by following the exact procedure as outlined above except for the addition of one step. This consists of rotating the horizontal beam plate holder and adjacent mirror a small precise amount between steps 5 and 6 above, i.e., between recording the test and the comparison scenes on the plate.

4.2 INTERPRETATION OF HOLOGRAPHIC INTERFEROGRAMS

Interpretation of both infinite fringe and finite fringe interferograms will be included in this section since both types of data will be acquired and analyzed during the course of this study.

The principle of operation of an interferometer is that optical interference occurs between two coherent beams passing through media of different density. Whenever optical paths are the same or differ by an integral multiple of λ, (where λ is the wavelength of the monochromatic light source. 6943A in this study) the beams reinforce one another whereas when a disturbance which shifts the optical path by any multiple of $\lambda/2$ is encountered, complete interference occurs. Complete reinforcement will show up as light fringes on a hologram plate and complete interference as dark fringes.

4.2.1 Infinite Fringe Interferograms

An example of an infinite fringe interferogram is presented in Figure 5. This horizontal view hologram was obtained with an unbroken one inch diameter helium bubble at a tank pressure of one atmosphere. Each fringe in this type of interferogram corresponds to a locus of constant optical path so interpretation for data reduction purposes consists of

numbering and locating the fringes along any plane of interest through the fireball. These fringe numbers and locations can directly be used to determine the integrated density or helium concentration change through the fireball along that optical path. Details of the computational procedure required to obtain concentration profiles from these fringe number data are presented in Section 5.1.3. In the sample infinite fringe interferogram presented, the density is constant inside the bubble and lower than the constant density region outside the bubble by about a factor of 7. Consequently, the interference fringes which consist of concentric circles with decreasing spacing as their radii increase depict only changes in optical path length through the helium sphere.

A second example of an infinite fringe interferogram is shown in Figure 7. This interferogram shows a vortex formed from an initial one inch diameter helium bubble at one atmosphere pressure after a rise of about 4 initial bubble diameters. The fringe pattern in this figure is more typical of that expected in this study in that the fringe geometry and spacing result from a toroidal cloud containing a mixture of helium and air.

One disadvantage of infinite fringe interferograms is that ambiguities can arise in reading the fringe numbers, particularly if the test event is turbulent. Since infinite fringe interferograms indicate the number of wavelengths that emitted light advances or is retarded in phase as it passes through the disturbance, it may not be apparent whether a fringe indicates an increase, decrease, or no change in fringe number. Unless there is an *a priori* knowledge of the flow field (obviously there is very little when the fireball is turbulent), ambiguities may occur. This fringe ambiguity problem can be eliminated by recording finite fringe interferograms which are described in the following section.

4.2.2 Finite Fringe Interferograms

An example of a finite fringe interferogram is presented in Figure 8. This interferogram was obtained at the same test conditions as the infinite fringe interferogram in Figure 7. In this type of hologram, the test disturbance causes a displacement or shift in the fringes relative to the undisturbed portion of the test section. An increase in optical

path is shifted in the opposite direction to a decrease in optical path, consequently no ambiguity car occur in regard to the fringe shift direction. The magnitude of the fringe shift in this type of hologram can be directly related to fringe number in an infinite fringe hologram and therefore to an integrated change in density or concentration along the optical path.

A second example of a finite fringe interferogram is presented in Figure 6. This hologram of another unbroken helium bubble was obtained at the same conditions as the infinite fringe interferogram of Figure 5. The spacing of the parallel fringes in this hologram is too large to allow the fringes to be just shifted as they were in Figure 7. Instead, several elliptic shaped fringes were formed near the top of the bubble. Although it is more difficult, even these fringes can be interpreted and the data reduced since the shift of each fringe will be relative to a specific determinable undisturbed fringe above the bubble. Finite fringe holograms with easier to reduce continuous fringes can be obtained in small events with high helium concentrations (such as this unbroken bubble) by increasing the amount of mirror and plate rotation between recording the test scene and comparison scene on the hologram plates.

One disadvantage of this form of hologram is that a visual picture including the outline of the test event is not obtained, however this is more than offset by the simplifications in the data reduction.

5. DATA REDUCTION

The purpose of this section is to describe briefly the technique for reducing holographic interferometry data as it applies to the present study. The process of achieving the final result, namely, determining the mean and fluctuating density field from the recorded holographic interferograms is comprised of two primary steps: first fringe interpretation, numbering and reading from the plates, and then computer data reduction of the density field. This approach has been used in a number of former studies (References 10, 11, and 12) which involved data reduction of both mean and fluctuating (turbulent) model reentry vehicle flow fields.

In each of the previous studies, density changes occurred as a result of pressure and temperature changes. In the present study, density changes result because of changes in molecular weight which occur when diffusion and mixing take place between helium and air at constant temperature and pressure. The interferometry measurements are basically measurements of the changes in the index of refraction field which is expressed in terms of both the mass fraction of helium, C_H, or air, C_A, and mass density, ρ. The perfect gas law can be expressed in terms of the same two unknowns and thus a solution for the species mass fraction and density can be obtained. The details to this approach for mean quantities is given in Section 5.1 while a discussion of the procedure for obtaining turbulent data is included in Section 5.2.

5.1 CALCULATION OF DENSITY PROFILES

5.1.1 Interferometry Theory

The standard equation for fringe shift is

$$S = \frac{1}{\lambda} \int_0^L (n - n_\infty)\, ds$$

where S = fringe number

λ = wave length of light in vacuum

L = integration path length

n = index of refraction

s = path length along the light ray

subscript

∞ = undisturbed conditions recorded in comparison scene and also observed in the test scene as a reference condition

The Abel inversion integral (discussed later in Section 5.1.2) is used to solve for n as a function of S for the case of axial symmetry. Here, one wants to consider how the solution $n - n_\infty$ can be used to calculate concentration or mass fraction profiles $C_i(r)$ from the interferograms.

For a multi-component gas case, the index of refraction becomes,

$$n = \sum K_i \rho_i + 1 = \rho \sum K_i C_i + = \rho \bar{K} + 1$$

where K = Gladstone-Dale constant

ρ = density

subscript

i = species i

superscript

$\bar{}$ = mean quantity

For helium and air (subscripts H and A, respectively)

$$n - 1 = \rho \{K_A C_A + K_H C_H\}$$

and because

$$\sum C_i = 1$$

$$\frac{n - n_\infty}{\rho_\infty K_\infty} = \frac{\rho K_A}{\rho_\infty K_\infty} \left[C_H \frac{K_H}{K_A} - 1) + 1\right] - 1 \qquad (1)$$

From the perfect gas law the density ratio, ρ/ρ_∞, may be obtained as

$$\frac{\rho}{\rho_\infty} = \frac{p}{p_\infty}\frac{T_\infty}{T}\frac{\bar{M}}{M_\infty}$$

where

T = temperature

p = pressure

M = molecular weight

A simplifying assumption, which in any event is non-crucial to the final results, is that $p = p_\infty$ and $T = T_\infty$, i.e., the pressure and temperature of the comparison and test scenes are the same. Then, $\rho/\rho_\infty = \bar{M}/M_\infty$.

From Dalton's Law of partial pressures,

$$p = T\sum \rho_i R_i = \rho T R \sum \frac{C_i}{M_i} = \rho T \frac{R}{\bar{M}}$$

where

R = gas constant per unit mass

R = gas constant per mole

and $\bar{M}$ is defined as

$$\frac{1}{\bar{M}} = \sum \frac{C_i}{M_i}$$

For helium and air,

$$\frac{1}{\bar{M}} = \frac{C_H}{M_H} + \frac{C_A}{M_A} = C_H\left(\frac{1}{M_H} - \frac{1}{M_A}\right) + \frac{1}{M_A}$$

Consequently the density ratio becomes

$$\frac{\rho}{\rho_\infty} = \frac{1}{C_H\left(\frac{M_\infty}{M_H} - \frac{M_\infty}{M_A}\right) + \frac{M_\infty}{M_A}}$$

The case here is for a comparison scene (sub ∞) comprised of air, thus

$$M_\infty = M_A \text{ and } K_\infty = K_A$$

and

$$\frac{\rho}{\rho_\infty} = \frac{1}{C_H\left(\frac{M_A}{M_H} - 1\right) + 1} \tag{2}$$

Eliminating ρ/ρ_∞ from equations (1) and (2) one obtains, after some algebra,

$$C_H = \frac{\frac{(n_\infty - n)}{\rho_\infty K_\infty}}{\left[\frac{(n - n_\infty)}{\rho_\infty K_\infty} + 1\right]\left(\frac{M_A}{M_H} - 1\right) - \left(\frac{K_H}{K_A} - 1\right)} \tag{3}$$

The mole fraction of helium becomes:

$$x_H = \frac{C_H \frac{M_A}{M_H}}{\frac{M_A}{\overline{M}}} \tag{4}$$

where

$$\frac{M_A}{\overline{M}} = C_H\left(\frac{M_A}{M_H} - 1\right) + 1$$

and the density ratio becomes

$$\frac{\rho}{\rho_\infty} = \frac{\overline{M}}{M_A} \tag{5}$$

The quantity $K_\infty \rho_\infty$ in Equation 3 is linearly dependent on pressure, and only slightly dependent on temperature and the wavelength of light used. A formula established by Biot and Arago expressing these dependencies and confirmed by more recent experiments (Reference 13) is

$$K_\infty \rho_\infty = n_\infty - 1 = \frac{n_0 - 1}{1 + \alpha T_\infty} p_\infty$$

where n_0 is the index of refraction at $T_\infty = 0°C$, $p_\infty = 1$ atm

α is the coefficient of thermal expansion in C^{o-1}

T_∞ is the ambient temperature in C^o

p_∞ is the ambient pressure in atmospheres

Values of n_0 and α required for this study were obtained from tables in Reference 13.

5.1.2 Abel Inversion and Numerical Integration

The basic interferometry equation which relates fringe number or fringe shift to the integrated change in index of refraction through a flow field is

$$S = \frac{1}{\lambda} \int_0^L (n - n_\infty) ds$$

where all quantities were defined in the previous section. Restricting consideration to an axisymmetric flow, the equation becomes

$$S(y) = \frac{1}{\lambda} \int_y^{r_0} (n - n_\infty) \frac{d(r^2)}{(r^2 - y^2)^{1/2}}$$

The new variables are defined in the figure below:

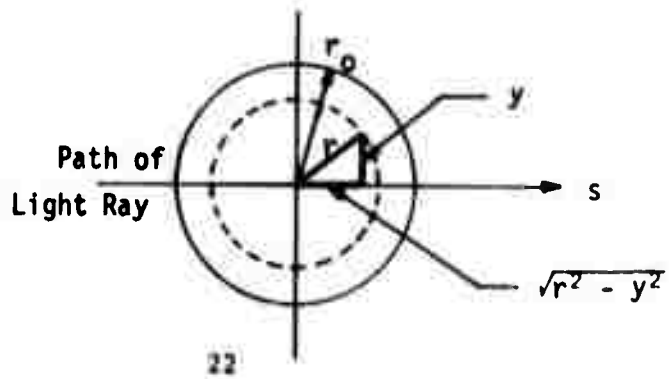

To solve for $n - n_\infty$, one notes that this equation is the same as Volterra's integral equation of the first kind, with the exception that the limits of integration are different. The details of the solution (Reference 14) are rather lengthy and will be omitted here. It becomes

$$(n - n_\infty)_{r=y} = -\frac{\lambda}{\pi}\int_y^{r_o} \frac{\frac{dS}{dr}\,dr}{(r^2 - y^2)^{1/2}} = -\frac{2\lambda}{\pi}\int_y^{r_N} \frac{dS}{d(r^2)}\,d(r^2 - y^2)^{1/2}$$

One can express this integral as a sum, (Reference 15),

$$(n - n_\infty)_{r=y_i} = \frac{2\lambda}{\Delta\pi}\sum_{\kappa=i}^{N-1} \frac{(S_\kappa - S_{\kappa+1})}{(2\kappa + 1)}\left\{[\kappa + 1)^2 - i^2]^{1/2} - (\kappa^2 - i^2)^{1/2}\right. \quad (6)$$

where $y_i = i\Delta$

Δ = zone width

$i = 0, 1, 2 \ldots N - 1$ (zones)

The calculation geometry is centered on the axis of symmetry and is comprised of N zones having constant properties as shown in the sketch:

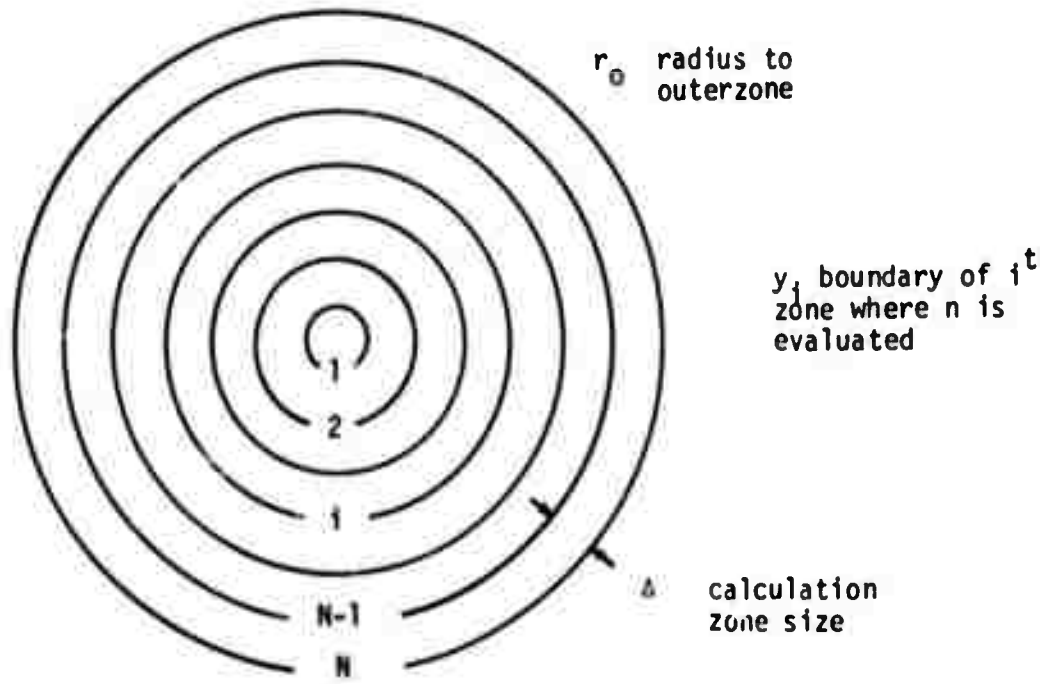

Having $n - n_\infty$ it is a simple matter with a computer program to calculate helium mole fraction, helium concentration, and density distributions using Equations 3, 4, and 5, respectively from Section 5.1.1.

5.1.3 Computational Procedure

Several steps are required in the data reduction procedure to obtain fringe number or fringe shift distributions necessary for input to the Abel Inversion computer program.

Photographs are obtained of the original 8 by 10 inch holographic plates (both horizontal and vertical views) yielding 4 by 5 inch negatives. These negatives are enlarged by a factor of approximately ten resulting in large scale positive transparencies. A horizontal plane coincident with the maximum diameter of each vortex is selected and identified by scribing a line on the working photographs. The light and dark fringes are located along each line and recorded. Fringes are then numbered starting with 1/2 for the outermost dark fringe (corresponding to the half wavelength shift in optical path discussed in Section 4.2), 1 for the next inward light fringe and so on, increasing by 1/2 each time a new fringe is encountered.* Next, the location of the vortex center is determined by the position of the minimum internal fringe number. These fringe number distributions for each half-vortex (having its origin at the vortex center) provide the input to a computer program which computes density, helium mole fraction, and helium concentration as functions of radial position.

To date, all data reduction has been performed following the procedure outlined above. The feasibility of automating the data reduction by digitizing each interferogram and analyzing the digital data with a sophisticated computer program is being studied. The DNA Film Digitizing Equipment at AFWL operated by ISI (see Reference 16) could

*Since many of the fringes appear as multiply connected regions, the same fringe may intersect the plane in question more than once. When this occurs, care must be taken to assign the same number to the same fringe.

possibly be used for this purpose. The primary difficulties at the present time are the software developments necessary, both in digitizing and analyzing the data.

5.2 CALCULATION OF TURBULENT STATISTICS

Data reduction of turbulent flows from holographic interferograms has been demonstrated for wakes in ballistic range firings (References 10 and 11). Various turbulent statistical quantities were calculated using a data reduction procedure developed especially for interferograms of hypersonic wakes (Reference 17). The main feature of this technique is that a cross view localization of the turbulent statistics is possible. Either by obtaining data at two angles from one hologram or by simultaneously obtaining data from two holograms recorded at different angles, these data, when cross correlated, can be shown to provide turbulent statistics localized in the vicinity of the intersection of the two views. It is anticipated that with a straightforward extension of this technique that at least some of the turbulent statistics of the rising fireball can be determined.

In this procedure, the holograms are first photographed from the desired view angle, the reconstructions accomplished using a cw laser. From the negatives, patterns of fluctuating optical density (indicative of change in fringe) are recorded by a microdensitometer. The extraction of the mean flow provides a new aspect to the data reduction due to the different structure of the fireball phenomena as compared to the turbulent wake. Once this operation has been accomplished, only fluctuations due to turbulence remain. These turbulent fluctuations provide the input to a fast Fourier transform computer program which was developed during the aforementioned wake studies. This program computes both the autospectrum and autocorrelation for each view, and the cross spectrum and cross correlation as well as an integral length scale for each pair of cross views.

In the future an attempt will be made to also obtain turbulent velocity fluctuation data using the particle tracking apparatus. Again the same approach must be used, namely extracting the mean velocity field from the data to yield only the turbulent components.

6. EXPERIMENTAL RESULTS

A discussion of both qualitative results from hardware development tests and reduced data from holographic interferograms obtained at both 4 and 8 atmospheres are presented in the sections below.

6.1 FACILITY DEVELOPMENT AND CHECKOUT EXPERIMENTS

Several preliminary tests were performed to support the development of the test facility, auxiliary hardware and diagnostic equipment. Fireball "size and rise" data obtained from shadowgraph motion pictures were used to establisn the size of the test tank and optical ports. These tests were performed at one atmosphere resulting in entrainment coefficients, (see Section 2.2), from 0.10 to 0.15 with an average value of 0.125*.

Additional shadowgraph data were obtained in the controlled test tank environment during the checkout phase of this equipment. A laser shadowgraph of a laminar vortex formed by the release of helium from a 2 inch diameter bubble at one atmosphere is presented in Figure 9. The Reynolds number** for this event is 3700. It is apparent from Figure 9 that the physics essential to toroid formation are contained within this experimental simulation. A turbulent vortex obtained with an initial helium bubble diameter of 1.1 inches and a tank pressure of 8 atmospheres corresponding to a Reynolds number of 12,300 is shown in Figure 10. The higher Reynolds number vortex in Figure 10 clearly shows both a large and small scale turbulent structure whereas the vortex in Figure 9 obtained at a lower Reynolds number is evidently laminar (i.e., appears to totally lack such structure). The evolution of a vortex from a sphere of helium at a high Reynolds number is shown as sequential frames of a shadowgraph motion picture film in Figure 11. It is interesting to note that structure identifiable on the periphery of

---

* These preliminary tests were performed in an uncontrolled environment (i.e., subject to air currents in a laboratory) which may account for some of the variation in the fireball growth rate.

**Reynolds number is defined as $Re = \rho_\infty u_T D_i / \mu_\infty$ where u_T is the terminal velocity of a non-entraining sphere, D_i is the initial bubble diameter, and ρ_∞ and μ_∞ are the ambient air density and dynamic viscosity, respectively.

the event is swept from the top around to the bottom and is either carried into the vortex because of circulation or trails to form a wake.

In addition to the preliminary experiments just described, numerous bench tests were conducted to investigate various remote soap bubble formation and bursting techniques which resulted in the development of the equipment described earlier in Section 3.1. Recent tests utilizing interferometry data obtained immediately after bubble breaking indicate that the capacitor discharge bursting system introduced initial asymmetries in the helium release which were not detected in the more qualitative shadowgraph data. A discussion of the possible effects of these asymmetries on the preliminary data is included in Section 6.2 while a recently developed initialization system which yields a symmetric helium release is described in Section 7.

6.2 HOLOGRAPHIC INTERFEROMETRY DATA

It should be noted that all preliminary fringe distribution and helium concentration results presented in this section are based on interferometry data obtained in tests in which the helium release was initiated with the electrode system described in Section 3.1. It is expected that the asymmetries attributed to this type of helium release will be considerably reduced through the use of the recently developed bubble breaking system described in Section 7.

6.2.1 Four Atmosphere Results

A total of twenty sets of holographic interferograms were obtained of different events at a tank pressure of four atmospheres. This tank pressure and the initial bubble diameter of one inch corresponds to a Reynolds number of 5500. Two such sets of interferograms are shown in Figures 12 and 13 for comparison purposes. The dark protuberance in the vertical views is the bubble tube below the vortex. The two vortices are approximately 3.5 and 4 inches in diameter, and both have risen about four initial bubble diameters. It is quite apparent that in general, the vortices are not identical in shape or symmetric in a given event. The

horizontal view of the vortex in Figure 12 is one of the more symmetric in appearance while that in Figure 13 is one of the more asymmetric.

Radial fringe number profiles for four typical vortex halves are shown in Figure 14 along with a mean distribution based on seven selected tests. The mean radial distribution of fringe numbers is depicted by the bold curve in the figure. The centers of the vortices were chosen to correspond to the minimum internal fringe, not to a tank fixed coordinate directly above the bubble tube. Presentation of the data in this manner tends to eliminate the effects of the larger scale motion (i.e., translational motion of the vortices).

A mean helium concentration profile for the 4 atmosphere data is presented in Figure 15. This profile was calculated from the mean fringe number distribution using the Abel Inversion program described in Section 5.1.2. The profile shows a helium concentration rapidly increasing from zero at the vortex edge ($r/r_0 = 1$) to a peak of about 1.3 percent at 0.75 of the normalized radius followed by a decrease to zero at about 0.25 of the vortex radius. The helium concentration becomes negative near the center of the toroid due to the assumption of axial symmetry inherent in the data reduction program.* When sufficient test results are acquired and averaged, they will produce a fringe distribution corresponding to a symmetric vortex and consequently will be compatible with the Abel Inversion procedure.

6.2.2 Eight Atmosphere Results

Ten sets of interferograms were acquired at a tank pressure of eight atmospheres. The Reynolds number for these events was 11,000 based on initial helium bubble diameters of one inch. One of the more symmetric events is shown in Figure 16. This vortex is approximately three inches

*It must be remembered from the governing equation for fringe shift that fringes in interferograms correspond to changes in index of refraction integrated along the path length of the light ray as it passes through the disturbance. The assumed axial symmetry invokes a prescribed path length dependent only on the diameter of the vortex and the radial position at which the helium concentration is to be calculated.

in diameter and has risen about five initial bubble diameters. It is obvious by comparing this event with the lower Reynolds number interferograms in Figures 12 and 13 that the higher Reynolds number fireball contains a greater amount of small scale turbulent structure. In addition, the fringes are closer together in the higher pressure events which combines to make the data reading and analysis far more difficult than in the lower pressure cases. With the present 8 atmosphere data, it is possible to number only the outermost fringes. Preliminary results from a mean of these outer fringe distributions were used to calculate a peak helium concentration level of slightly over one percent for the 8 atmosphere test condition. Improvements in the holographic reconstruction technique and possibly the use of hydrogen as a replacement for helium in the experiments are currently being studied as means of improving the fringe resolution for the high pressure tests.

It is important to realize that fringe shifts in an interferogram of a turbulent event result from a combination of both a mean and fluctuating density field integrated along the light path. As a consequence, a large sample of data obtained at the same test conditions must be ensemble averaged so that smaller scale asymmetries due to turbulence will be averaged out. A valid mean density profile can then be calculated with the Abel Inversion program since the inherent requirement of axial symmetry will be satisfied. Statistical studies are now in progress to establish the number of data samples necessary to achieve desired levels of accuracy in the reduced helium concentration profiles. It is now quite apparent that 50 to 100 or more sets of repeat data will be required at each test condition of interest.

7. CURRENT STATUS AND FUTURE PLANS

A recent major effort has been directed towards improving the bubble breaking technique thought to be the primary cause of the larger asymmetries in the simulated fireballs. Several different electrical discharge and mechanical devices were tested including the use of multiple electrodes, but none produced satisfactory results. A mechanical breaking technique of dropping a small metal sphere through the top of the bubble has repeatedly produced a symmetric helium release in tests at one atmosphere.

An interferogram obtained using this technique is presented in Figure 17. This interferogram was obtained several milliseconds after the bubble was broken and shows the sphere just above the bubble tube. As a basis of comparison, a typical early time interferogram obtained using a single electrode breaker is shown in Figure 18. The improvement obtained with the new bubble bursting technique is obvious. Two additional interferograms that were obtained with this technique were presented earlier in Section 4 as Figures 7 and 8.

The prototype equipment to check this bubble bursting concept used 125 mil diameter spheres and did not allow the test tank to be pressurized. Equipment is currently being fabricated for the remote feed and release of smaller 40 mil diameter steel spheres from the top of the test tank. Once this new equipment is installed and tested, over 50 repeat sets of both interferometry and particle tracking data will be acquired at the 4 atmosphere test condition described in Section 6.2.1. Repeat sets of similar data will then be obtained at 8 and 10 atmospheres pressure and finally at 10 atmospheres pressure in an SF_6 environment to provide an additional increase in Reynolds number.

Atmospheric simulation tests will also be performed by rapidly reducing the tank pressure with the vent system while the torus is formed and rises. In this phase of the experiments the effect of fireball expansion resulting from pressure variation with altitude will be simulated. However, the effect of stratification or atmospheric scale height will not be simulated in the currently planned experiments.

The emphasis in the data reduction and analysis will initially be oriented towards ensemble averaged data and determination of fireball mean velocity and density characteristics. With this data base established, attention will then be focused on the primary subject of the study, a determination of the fireball turbulent field and its effect on entrainment and mixing.

REFERENCES

1. Wang, C. P., "Motion of an Isolated Buoyant Thermal," The Physics of Fluids, Vol. 14, No. 8, pages 1643-1647, August 1971.

2. Morton, B. R., Taylor, Sir Geoffrey, and Turner, J. S., "Turbulent Gravitational Convection from Maintained and Instantaneous Sources," Proc. Roy. Soc., Vol. A 234, pages 1-23, January 1956.

3. Walters, J. K., and Davidson, J. F., "The Initial Motion of a Gas Bubble in an Inviscid Liquid," Journal of Fluid Mechanics, Vol. 17, pages 321-336, 1963.

4. Maxworthy, T., "The Structure and Stability of Vortex Rings," Journal of Fluid Mechanics, Vol. 51, Part 1, pages 15-32, January 1972.

5. Fohl, T. and Murphy, B. L., "Interaction between Buoyantly Rising Fireballs (U)," Mt. Auburn Research Report No. MARA-SRD-121, DASA 2483, April 1970, Secret Restricted Data.

6. Fohl, T. and Zalay, A. D., "Modelling of Flow of Low Altitude Fireballs (U)," Mt. Auburn Research Report No. MARA-SRD-149, DASA 2644, February 1971, Confidential Formerly Restricted Data.

7. Witte, A. B., "Three Dimensional Flow Field Analysis by Holographic Photography and Interferometry," Final Technical Report, No. 12414-6003-RO-00, 15 November 1969.

8. Bourot, J. M., Chronophotographie des champs aérodynamiques. Publs. sci. et tech. Ministère Air, France, 226, 1949. Also Bourot, J. M. and Moreau, J. J., Méchanique des fluides-Sur la visualisation du tourbillon marginal d'une aile, au moyen de lamelles d'aluminum, en soufferie aérodynamique. Compt. rend. 228, 1567-1569 (1949); Méchanique des fluides-Note sur les zones d'inégale luminosité observées dans certaines visualisationd d'éncoulements. Compt. rend. 228, 1628-1630 (1949).

9. Hale, R. W., et al, "Experimental Investigation of Several Neutrally Buoyant Bubble Generators for Aerodynamic Flow Visualization," Sage Action Inc., Naval Research Reviews, pages 19-24, June 1971.

10. Witte, A. B. and Wuerker, R. F., "Laser Holographic Interferometry Study of High-Speed Flow Fields," AIAA Paper No. 69-347, AIAA 4th Aerodynamic Testing Conference, April 1969.

11. Witte, A. B., Fox, J., and Rungaldier, H., "Localized Measurements of Wake Density Fluctuations Using Pulsed Laser Holographic Interferometry," AIAA Paper No. 70-727, AIAA Reacting Turbulent Flows Conference, June 1970.

12. Witte, A. B., Fox, J. and Rungaldier, H., "Holographic Interferometry Measurements of Mean and Localized Fluctuating Wake Density Field for Cones Fired at Mach 6 in a Ballistic Range," AIAA Paper No. 71-564, AIAA 4th Fluid and Plasma Dynamics Conference, June 1971.

13. Forsythe, W. E., ed., "Smithsonian Physical Tables," 9th Edition, Tables 533-534, pages 532-533, 1954.

14. Weyl, F. J., "Analytical Methods in Optical Examination of Supersonic Flow," NAVORD Report No. 211-45, Bur. Ordnance, Navy Department, 11 December 1945.

15. Gooderum, P. B. and Wood, G. P., "Density Fields Around a Sphere at Mach Numbers 1.30 and 1.62," NACA-TN-2173, August 1950.

16. Dudziak, W. F., Devan, D. I., and Anderson, G. C., "Annual Summary Report: DNA Optical Data Reduction and Analysis Facility," Information Science, Inc. Report No. 11087, November 1971.

17. Fox, J., "Statistical Analysis of a Turbulent Wake by Means of Laser Hologram Interferometry," TRW Report No. 12414-6002-RO-00, June 1969.

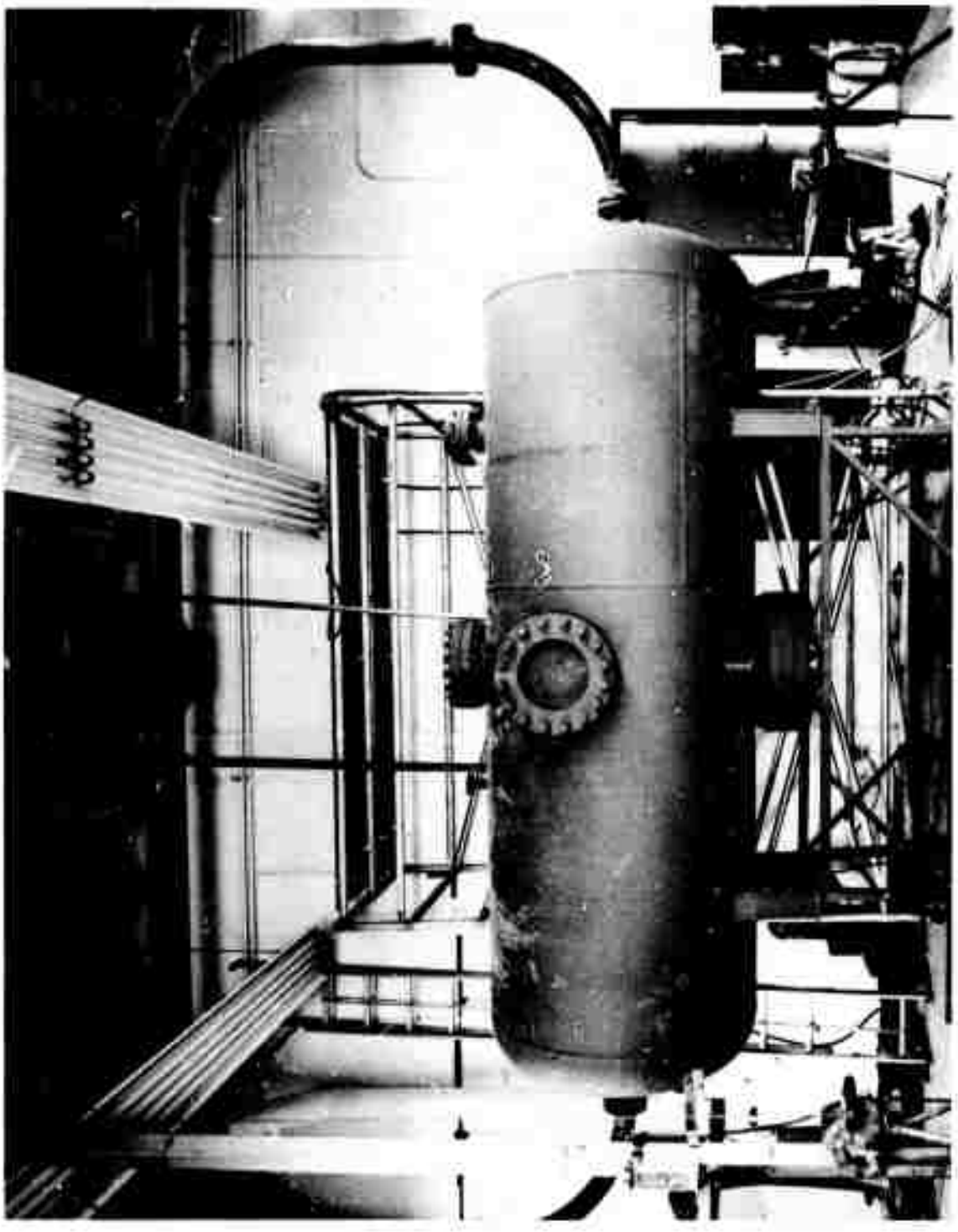

Figure 1. High Pressure Test Tank and Vent System

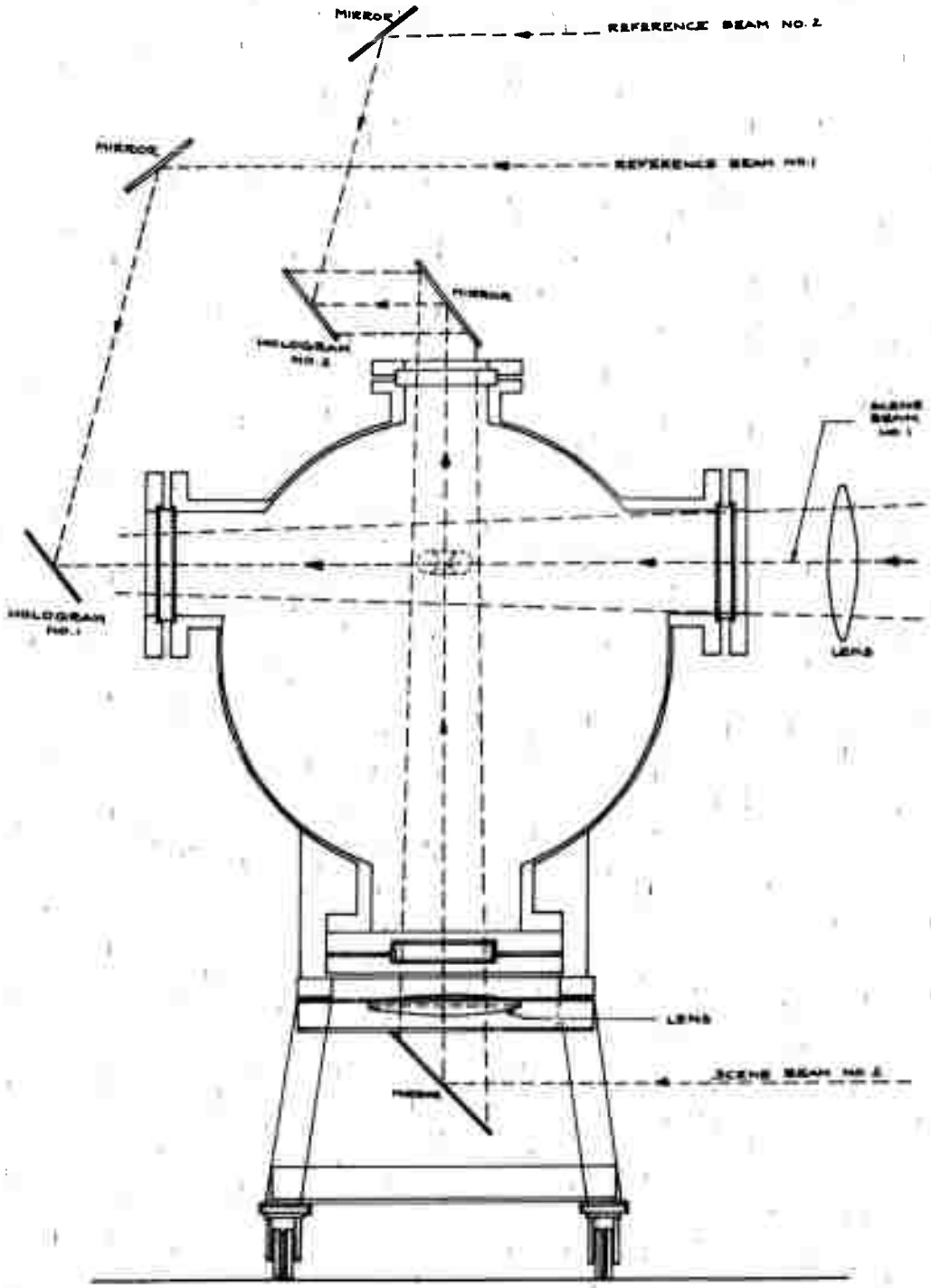

Figure 2. Test Tank Cross-section and Nearby Holocamera Components

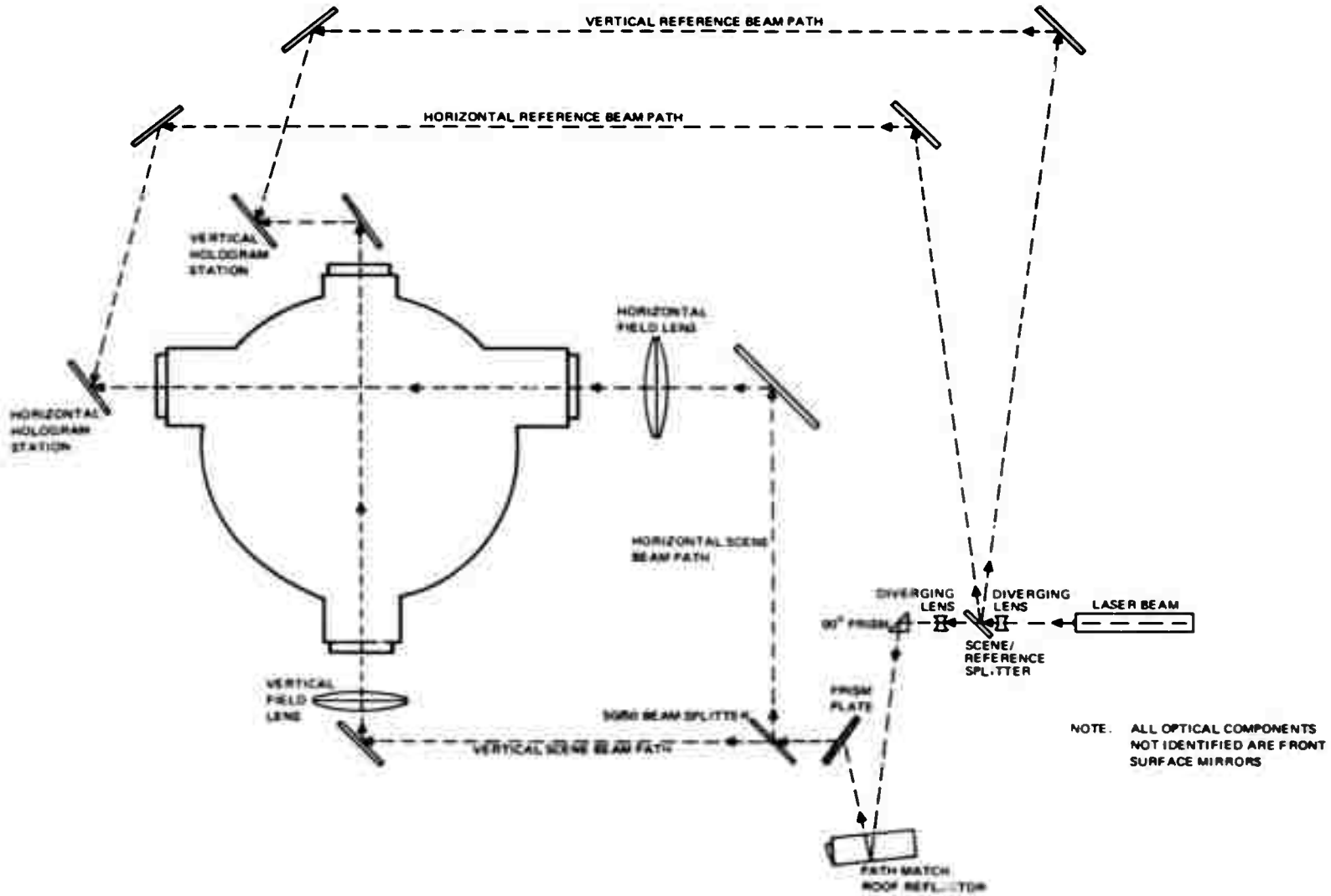

Figure 3. Schematic Diagram of Holocamera

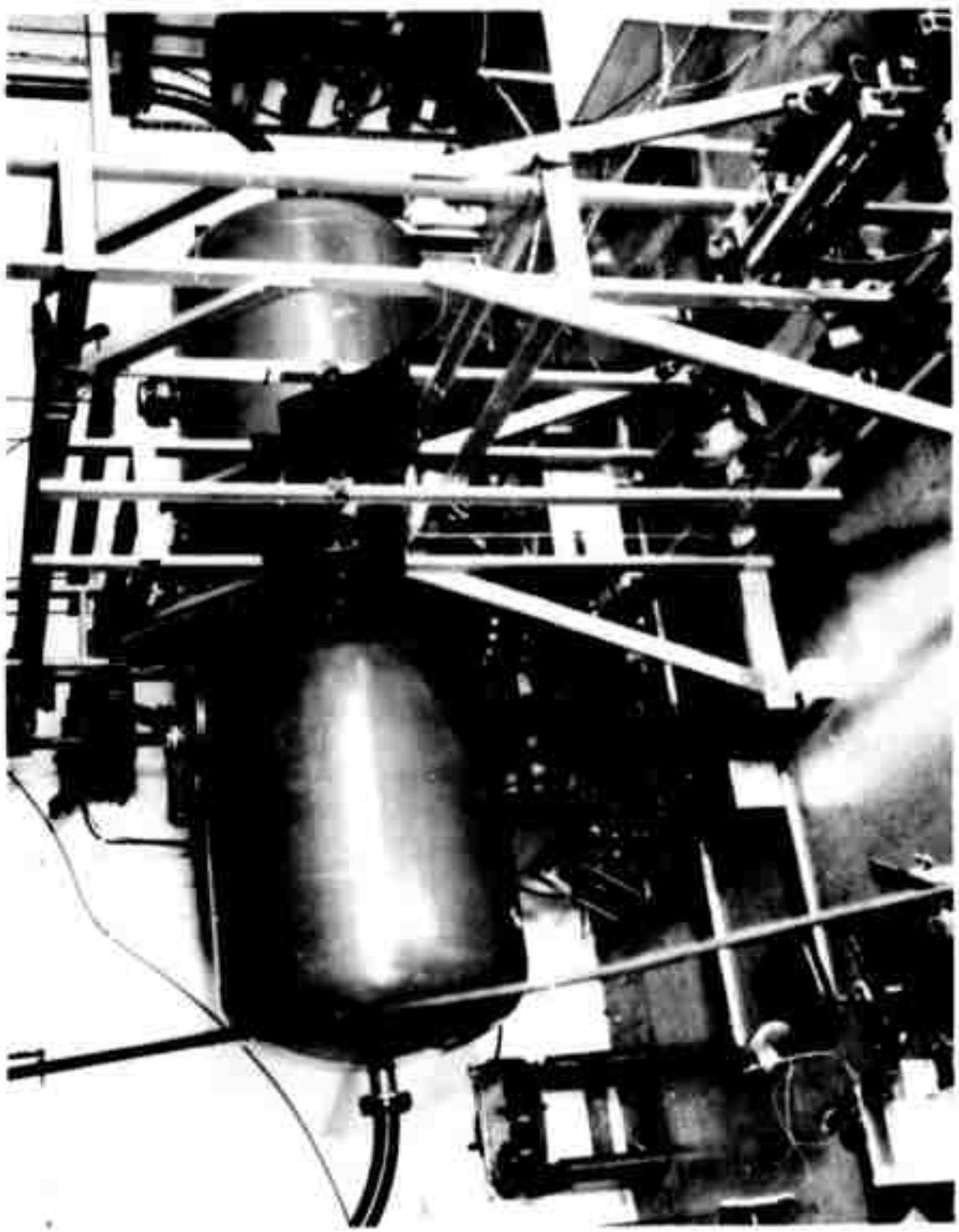

Figure 4. Photograph of Tank and Holocamera Arrangement

Figure 5. Infinite Fringe Interferogram of Helium Filled Soap Bubble

Figure 6. Finite Fringe Interferogram of Helium Filled Soap Bubble

Figure 7. Infinite Fringe Interferogram of Bubble Shortly after Bursting

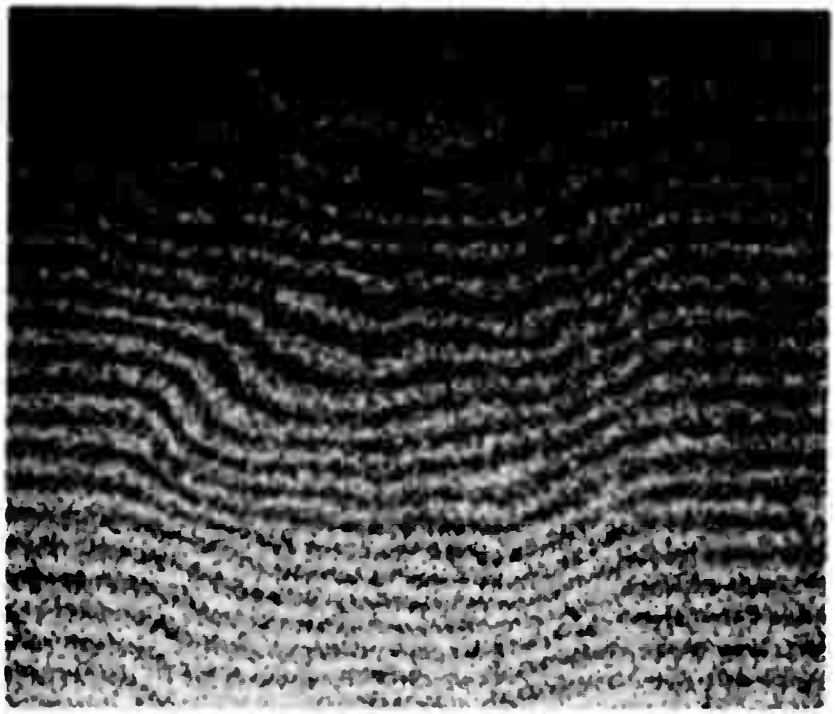

Figure 8. Finite Fringe Interferogram of Bubble Shortly after Bursting

Figure 9. Shadowgraph of Laminar Vortex

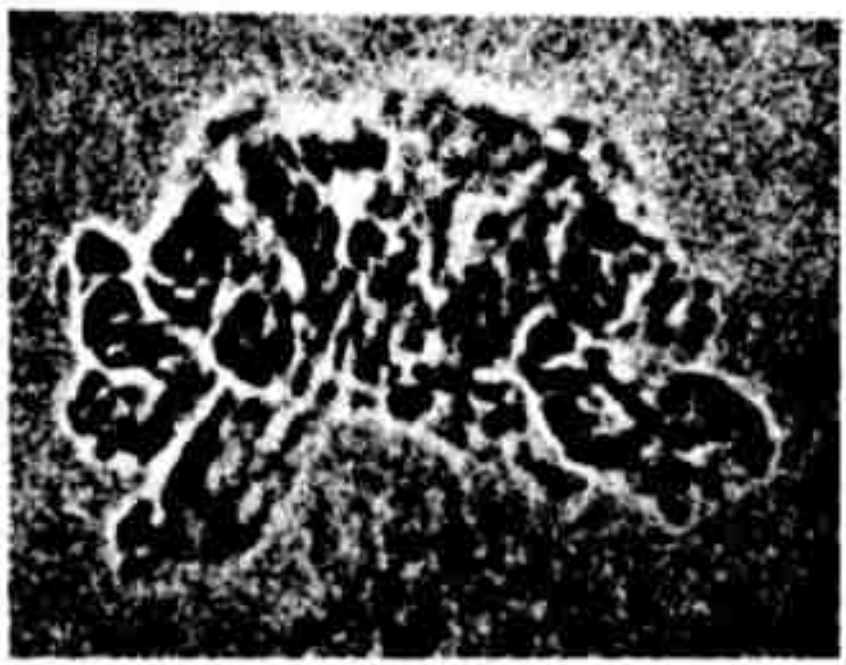

Figure 10. Shadowgraph of Turbulent Vortex

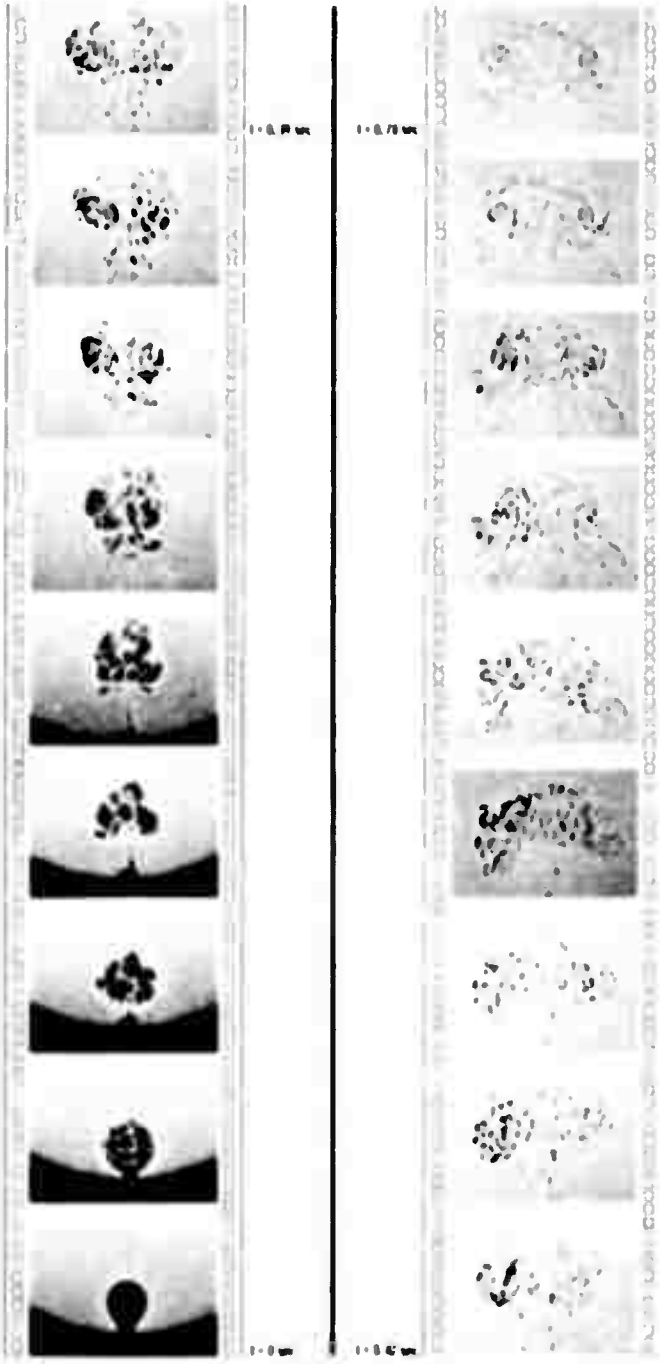

Figure 11. Shadowgraph of Turbulent Vortex Evolution from Helium Bubble

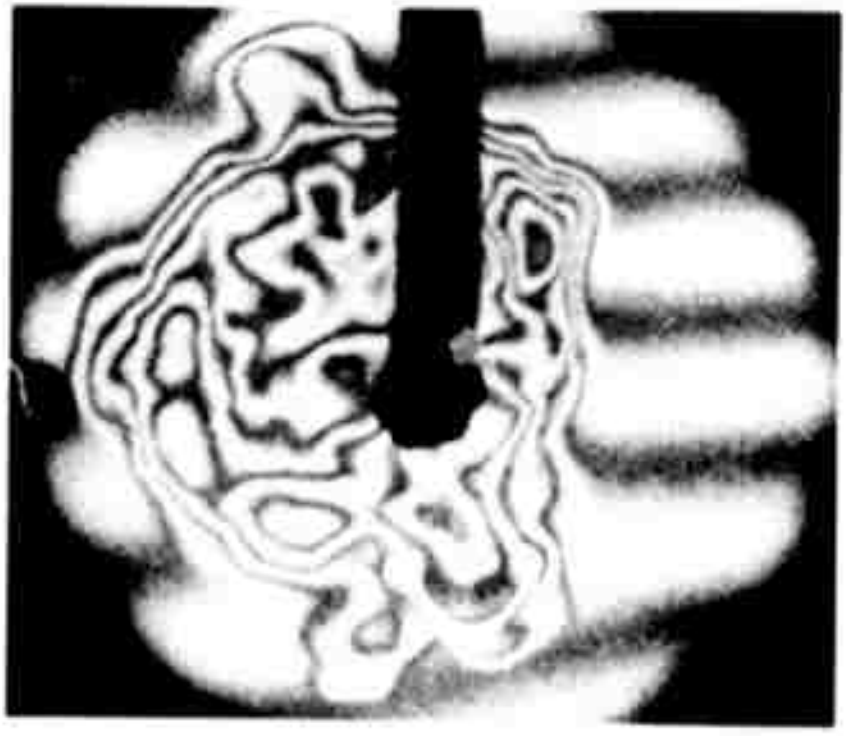

Vertical View

Horizontal View

Figure 12. Infinite Fringe Interferogram of 4 Atmosphere Vortex

Vertical View

Horizontal View

Figure 13. Infinite Fringe Interferogram of 4 Atmosphere Vortex

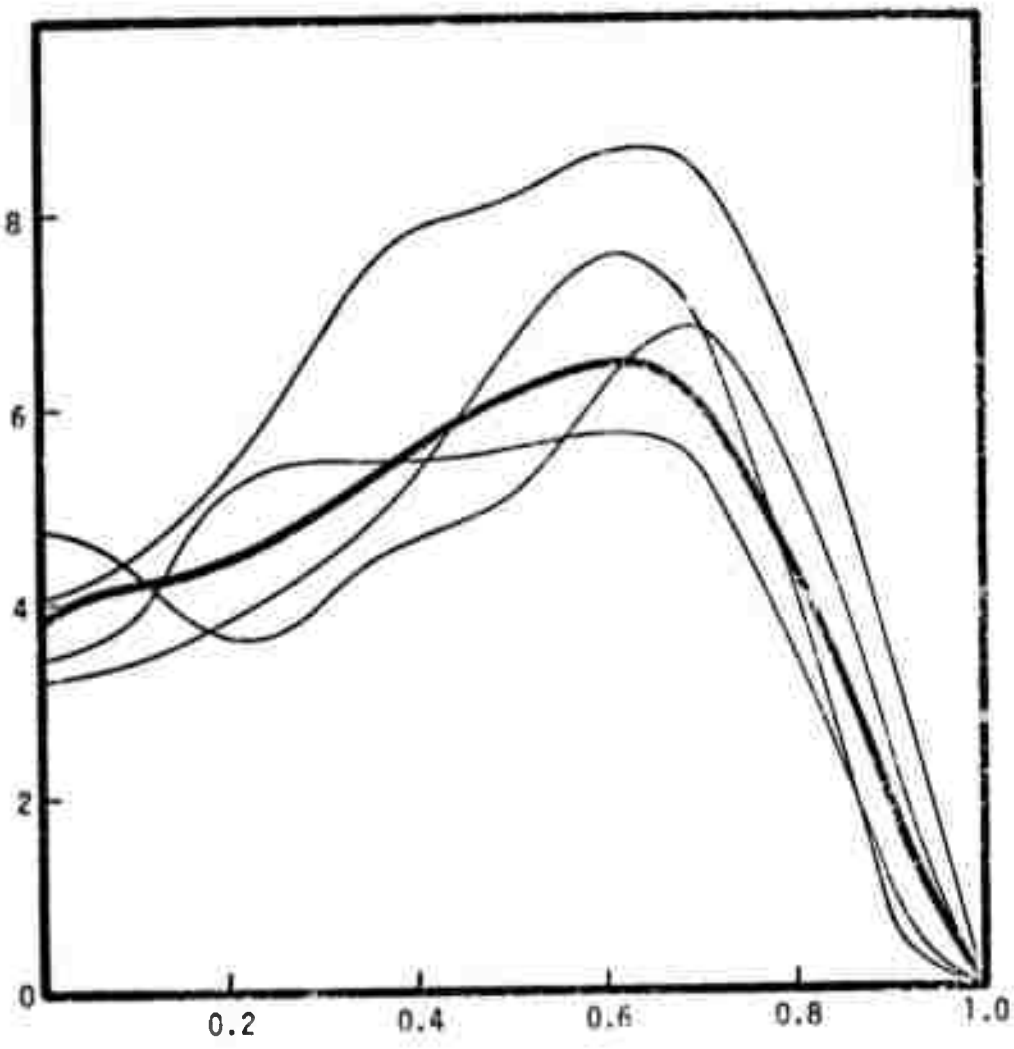

Figure 14. Radial Fringe Number Distributions - Typical 4 Atmosphere Events and Average

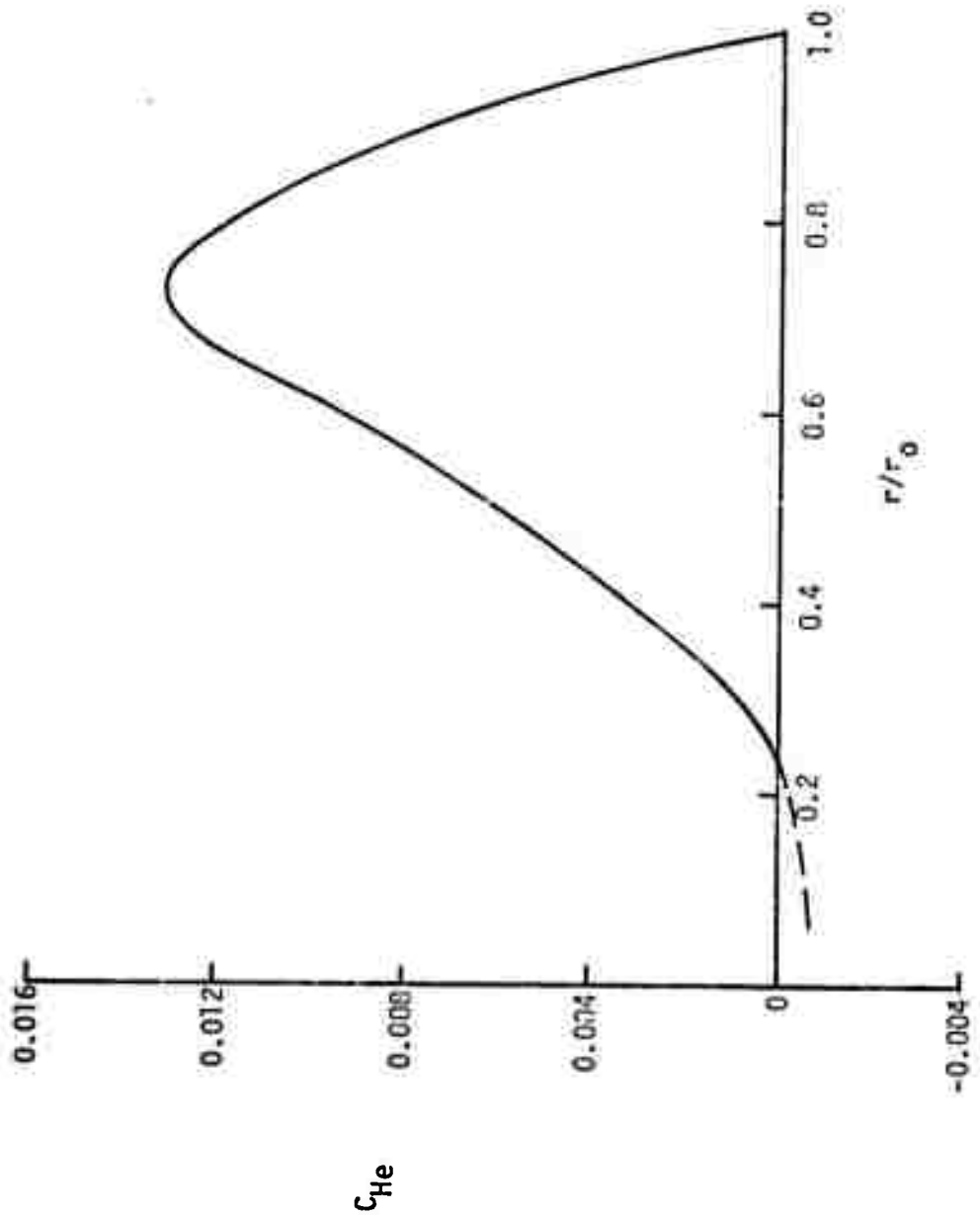

Figure 15. Radial Helium Concentration Profile - Averaged 4 Atmosphere Data

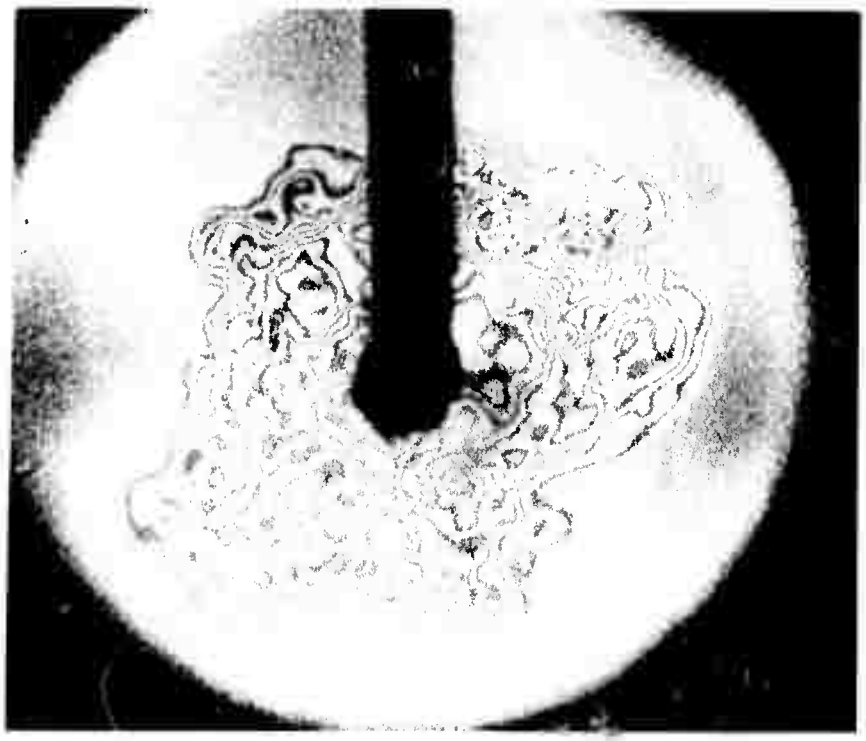

Vertical View

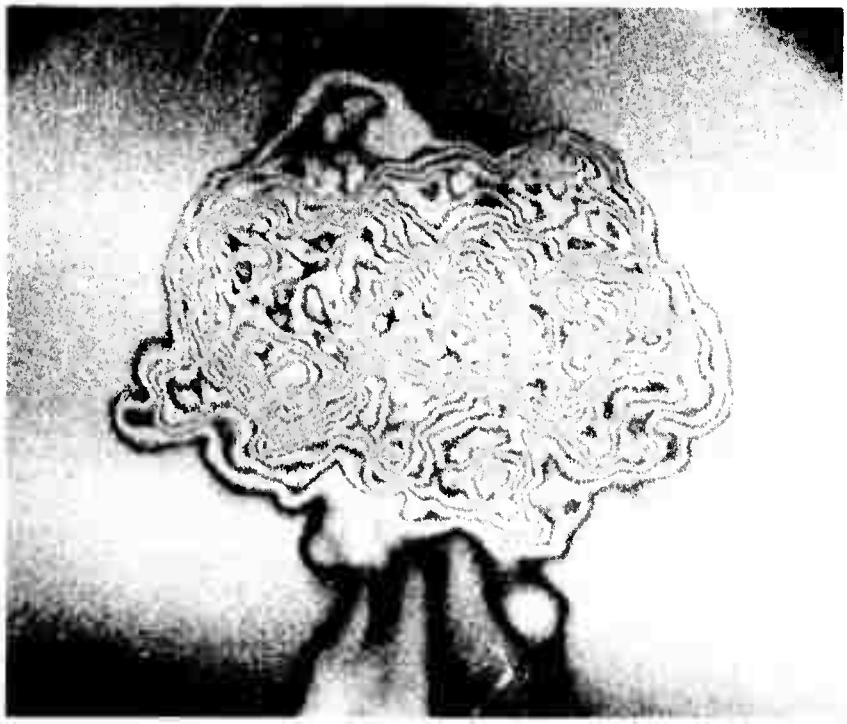

Horizortal View

Figure 16. Infinite Fringe Interferogram of 8 Atmosphere Vortex

Figure 17. Interferogram of Helium Release - Sphere Dropping Technique

Figure 18. Interferogram of Helium Release - Electrode Technique